Discovery of anti-SARS-CoV-2 molecules using structure-assisted repurposing approach targeting N-protein

Preeti Dhaka[1], Ankur Singh[1], Shweta Choudhary[1], Pravindra Kumar*[1], Gaurav Kumar Sharma*[2], Shailly Tomar*[1]

[1] Department of Biosciences and Bioengineering, Indian Institute of Technology Roorkee, Roorkee, Uttarakhand - 247667, India
[2] Indian Veterinary Research Institute, Izatnagar, Bareilly, Uttar Pradesh state - 243122, India

Corresponding authors*

***Shailly Tomar**
Professor,
Department of Biosciences and Bioengineering,
Indian Institute of Technology Roorkee,
Uttarakhand (247667), India
Email: shailly.tomar@bt.iitr.ac.in

***Gaurav Kumar Sharma**
Senior scientist
Indian Veterinary Research Institute,
Izatnagar, Bareilly,
Uttar Pradesh state (243122), India
Email: gaurvet@gmail.com

***Pravindra Kumar**
Professor,
Department of Biosciences and Bioengineering,
Indian Institute of Technology Roorkee,
Uttarakhand (247667), India
Email: pravindra.kumar@bt.iitr.ac.in

Abstract

SARS-CoV-2 nucleocapsid protein (N-protein) is a virus specific multitasking protein, responsible for recognition and encapsidation of the viral genome. The N-terminal domain (NTD) of N-protein has a major role of packaging viral RNA genome into a long helical nucleocapsid structure. In this study, using structure-based drug repurposing strategy, small molecules from a FDA approved, natural product, and LOPAC^{1280} libraries have been virtually screened against the RNA binding pocket of SARS-CoV-2 NTD and twelve candidate molecules with high binding affinity were identified. Highly sensitive isothermal titration calorimetry (ITC) method was utilized to confirm binding of these molecules to purified NTD protein. *In vitro* cell-based SARS-CoV-2 antiviral assays demonstrate that nine of these identified molecules are highly efficacious in inhibiting virus replication with half maximal effective concentration (EC_{50}) ranging from 0.98 µM-10 µM. FDA approved drugs: Telmisartan, an angiotensin II type 1 (AT1) receptor antagonist used in the management of hypertension and Bictegravir, an HIV-1 integrase inhibitor showed significant inhibitory activity against SARS-CoV-2 with a EC_{50} values of 1.02 µM and 8.11 µM respectively. Additionally, Bisdemethoxycurcumin, a natural analogue of curcumin and MCC-555, an anti-diabetic drug exerted antiviral activity with EC_{50} values of 1.64 µM and 4.26 µM, respectively. Taken together, this is the first report of drug molecules targeting the NTD of SARS-CoV-2 N-protein and the data presented in this study exhibit high potential for development of COVID-19 therapy based on drug repurposing.

Keywords: SARS-CoV-2, Nucleocapsid, RNA binding domain, Drug repurposing, Antivirals

Introduction:

The pandemic of Coronavirus Disease 2019 (COVID-19) caused by the Severe acute respiratory syndrome coronavirus 2 (SARS-CoV-2) and the increased frequency of new variants emergence has created a situation of havoc worldwide from past few years. SARS-CoV-2 is an enveloped positive-sense single-stranded RNA virus (ss RNA) of the *Coronaviridae* family[1]. The spherical-shaped SARS-CoV-2 shares approximately 50-80% similarity with other coronaviruses such as MERS (Middle East Respiratory Syndrome), SARS-CoV (Severe acute respiratory syndrome coronavirus), and bat coronaviruses[2,3]. Irrespective of other coronaviruses, SARS-CoV-2 is highly infectious and fatal. The disease was first reported in December 2019 in Wuhan, China[4]. Since then, it has been widespread and has challenged the economy and healthcare systems worldwide. As of March 2022, the pandemic has severely affected ~440 million people and caused mortality of over 6 million people globally[5]. Early-stage clinical symptoms of COVID-19 are dry cough, fever, and fatigue[6]. In more severe cases, the infection can cause pneumonia, organ dysfunction, acute respiratory distress syndrome (ARDS), cardiac injury, and sometimes death[6,7].

SARS-CoV-2 contains ~30 kb polyadenylated and capped genome that is one of the largest genome among RNA viruses[7]. Its genome comprises fourteen open-reading frames (ORFs) with an arrangement of the following order: 5'-ORF1a-ORF1b-S-ORF3-E-M-N-3' including some accessory factors such as 3a-3b, 6, 7a-7b, 8, 9b-9c, and 10[8–10]. ORF1a and ORF1b encode two polyproteins (pp1a and pp1ab) cleaved by viral proteases into functional non-structural proteins (nsp1-16)[10,11]. These nsps play crucial roles in viral replication through their enzymatic functions. The remaining ORFs encode subgenomic (sg) mRNAs and accessory factors[11]. The sg mRNAs further translate to produce four structural proteins; spike (S), envelope (E), membrane (M), and nucleocapsid (N-protein), along with some accessory factors[12]. These proteins help in the entry and survival of virus inside the host cell.

In positive-sense RNA viruses, multifunctional N-protein plays pivotal roles at different stages of the viral life cycle, such as regulation of the viral RNA replication/transcription, alteration of host cells metabolism, viral budding, and assembly[13–16]. The N-protein primarily interacts with the viral RNA and provides stability by packaging the genome into a helical ribonucleoprotein (RNP) structure[17,18]. The N-protein in SARS-CoV-2 entails two functional domains: the N-terminal RNA encapsidation domain (residues 46-174) and the C-terminal oligomerization domain (residues 247-364) that are linked through a disordered stretch of Ser/Arg (SR)-rich central linker region (residues 180-247)[17,19–22]. Studies on SARS-CoV-2 N-protein suggest that its NTD is highly conserved and shares structural and functional similarities with other coronaviruses such as Human coronavirus OC43 (HCoV-OC43), Mouse Hepatitis Virus (MHV), MERS, and SARS-CoV. Additionally, the three dimensional (3D) structural characterization of SARS-CoV-2 NTD suggests that it folds like a right-hand structure with a hydrophobic palm, basic fingers, and a wrist made up of acidic residues[23]. The flexible NTD with aromatic and positively charged residues form a basic RNA binding groove that neutralizes the phosphate groups on RNA[18]. The exposed aromatic residues of the hydrophobic palm contact the base moieties to bind with the viral RNA[18,24,25]. NTD shows hydrophobic and electrostatic interactions with viral RNA and packs them into a complex of RNP. Previous crystal structure studies of the NTD-N protein of coronaviruses provide a clear understanding about the binding of RNA, nucleotides, and inhibitors in the RNA binding pocket of NTD[26–28]. The RNA binding pocket of SARS-CoV-2 NTD of the N-protein comprises Ser52, Phe54, Ala56, Ala91, Arg108, Tyr110, Tyr112, and Arg150 and is accountable for encapsidation of the viral RNA[25,26,29]. Targeting this pocket is expected to hinder the binding of viral RNA with the N-protein. Therefore, NTD is a potential target for the identification of new therapeutic interventions against SARS-CoV-2 infection.

For a molecule to concrete its character as a drug into the pharmaceutical market, it has to endure several pre-clinical and clinical trial processes that are highly expensive and time taking approaches. To lay off these approaches, there is an utmost need to find quick and effective alternatives from available compound libraries against the upcoming and widespread diseases[30]. With the introduction of bioinformatics, the repurposing of molecules is now at ease than earlier[31]. To fasten the process of drug discovery, various drug libraries are commercially available for structure-based, biochemical, and *in vitro* screening against target proteins. The present study focuses on structure-based identification and *in vitro* evaluation of small molecules targeting the NTD of N-protein to identify existing small molecule drugs that harbour antiviral activity against SARS-CoV-2. Using this approach, twelve compounds were identified from three different compound libraries [Food and Drug Administration (FDA) approved drug library[32], natural compounds[32], and Library of pharmacologically active compounds (LOPAC[1280])[33]] that displayed high binding affinities against the NTD of SARS-CoV-2 N-protein. The selected compounds were further evaluated for their binding affinities through biophysical characterisation studies, and their antiviral efficacy was assessed using *in vitro* cell culture-based assays.

Material & Method:

Production of SARS-CoV-2 NTD:

The gene fragment of NTD (residues 1-174) was PCR amplified using the template plasmid received from National Centre for Cell Science (NCCS), Pune (a kind gift from Dr Janesh Kumar). The two sets of oligonucleotide primers 5'-ATATGGCTAGCCGGCCCCAAGGTTTACCCAATAATACTGC-3' (forward) having NheI restriction site & 5'-AAGCTTGTCGACTTATTCTGCGTAGAAGCCTTTTGGCAA-3' (reverse) having SalI restriction site were designed to amplify NTD of SARS-CoV-2 N-protein. The PCR product was digested with NheI and SalI enzymes and subsequently ligated into the pET28c vector using DNA ligase. The competent *E. coli* DH5α cells were transformed with the recombinant plasmid using $CaCl_2$ heat shock method, followed by plasmid isolation and confirmation of the gene insert through DNA sequencing. The recombinant plasmid containing the NTD gene fragment was transformed into the Rosetta (DE3) strain of *E. coli.* The transformed Rosetta cells were inoculated in Luria-Bertani broth, containing 35 μg/ml chloramphenicol and 50 μg/ml kanamycin, and the culture was grown at 37 °C until optical density reached 0.6 at 600 nm (OD600). The expression of NTD was induced by adding 0.35 mM isopropyl β-d-1-thiogalactopyranoside (IPTG), and the cells were allowed to grow at 18 °C for 16 h. The bacterial cells were harvested by centrifuging the culture at 6000 rpm at 4 °C for 10 min. The pellet was re-suspended in lysis buffer (50 mM Tris, 250 mM NaCl, pH-7.5). Cells were disrupted using French press (Constant Systems Ltd., Daventry, England) at 21 kpsi pressure followed by high-speed centrifugation of the cell lysate at 12000×*g* for 1.5 h at 4 °C. The supernatant was loaded onto a pre-equilibrated nickel-nitrilotriacetic acid (Ni-NTA) column (BioRad, India). Subsequently, the column was washed with different concentrations of imidazole (10 mM and 50 mM) in wash buffers, and the protein was eluted with 300 mM imidazole. The molecular weight and purity of the 6xHis-tagged NTD protein were observed on sodium dodecyl sulphate–polyacrylamide gel electrophoresis (SDS-PAGE). The estimated molecular weight of the protein was 21.7 kDa (Figure SF1). The protein was dialysed using

1XPBS buffer (137 mM NaCl, 2.7 mM KCl, 4.3 mM Na_2HPO_4, 1.47 mM KH_2PO_4, pH 7.3) overnight at 4 °C. The dialysed protein was concentrated to ~3.6 mg/ml using Ultra-15 Amicon (Millipore, USA) with a 10-kDa cut-off. The protein concentration was estimated using the extension coefficient method at wavelength 280 nm.

Molecular docking of Guanosine monophosphate (GMP) into the RNA binding pocket:

Multiple sequence alignment (MSA) of SARS-CoV-2 NTD with the NTD from SARS-CoV, MERS-CoV, and HCoV-OC43 coronaviruses illustrates the residues involved in interaction with GMP in the RNA binding pocket are primarily conserved. The MSA was done using MultAlin software[34], and the image was processed using ESPript 3.0[35]. To gain deeper insights into the structural similarities of NTD among coronaviruses, the crystal structures downloaded from Protein Data Bank (PDB) were used as a template. The structural superimposition of SARS-CoV-2 (PDB ID: 6M3M)[25] with SARS-CoV (PDB ID: 2OFZ)[28], MERS-CoV (PDB ID: 4UD1)[24], and HCoV-OC43 (PDB ID: 4KJX, 4LI4, 4LM9)[26] was performed using PyMol[36]. For molecular docking study, the atomic structure of SARS-CoV-2 NTD (PDB ID: 6M3M)[25] was retrieved from RCSB-PDB and three-dimensional structure of GMP was extracted from the PubChem database. The protein structure was refined by removing water molecules followed by addition of Kollman charge (8.0) and polar hydrogen atoms. GMP structure was prepared by adding Gasteiger charge (0.5203) and polar hydrogen atoms on it. The refined protein and GMP were further saved in the .pdbqt file. The grid box for docking of GMP was prepared by covering the key RNA binding residues in the NTD of SARS-CoV-2 N-protein (Ser52, Phe54, Ala56, Ala91, Arg108, Tyr110, Tyr112, and Arg150) with dimensions 44Å×46 Å×43Å, and centre point coordinates X= 13.566, Y= -6.239, and Z= -18. The Lamarckian genetic algorithm was used to calculate the 10 conformations of GMP with the maximum number of evaluations (250,000,000) by setting other parameters as default. The AutoDock Tools[37] and AutoDock vina[38] were used for the docking study. The best-fitted conformation of GMP with NTD was carefully picked based on binding energy (B.E.), and root mean square deviation (RMSD) value. The molecular interaction of NTD-GMP complex was evaluated using PyMol[36] and LigPlot[39].

Virtual screening and molecular docking of compound libraries:

For structure-based virtual screening of small molecules against NTD, PyRx 0.8[40], and AutoDock tools/Vina[37,38] platforms were used. PyRx 0.8 platform was used to screen the compounds of LOPAC[1280], Natural compound library, and FDA approved drug library against the conserved RNA binding pocket of NTD (PDB ID: 6M3M). The FDA and natural product library were downloaded from the Selleckchem database, and the LOPAC[1280] library was purchased from Sigma Aldrich. Ligands were first energy minimized and then converted from SDF format to Autodock ligands (.pdbqt) format using inbuilt OpenBabel software in PyRx 0.8. Subsequently, the aforementioned grid box dimensions of the NTD-GMP complex were used for virtual screening and molecular docking studies by keeping other parameters as default.

Previous reports showed that the inhibitor (PJ34) against the GMP binding site of NTD of HCoV-OC43 reduced RNA-binding affinity and the viral replication significantly. The molecular docking of the best fit conformation of PJ34 revealed the B.E. -6.2 kcal/mol. Keeping the B.E. of NTD-GMP and NTD-PJ34 complex as reference, top hit molecules were further selected for detailed docking studies. For molecular docking, water molecules were removed from the crystal structure. The structure of NTD protein was prepared for docking by adding Kollman charges (8.0) and polar hydrogen atoms using AutoDock tools. The .pdbqt file format of top hit ligands was retrieved from the PyRx directory and processed by adding Gasteiger charges and polar hydrogen atoms. The protein and ligands were saved in .pdbqt file format, and molecular docking of ligands was performed similar to docking of GMP against NTD. The best conformations of the ligands were selected based on interactions with NTD, RMSD values, and their binding energies. The selected NTD-ligand complexes were analysed using PyMOL[36] and LigPlot[+39].

Isothermal Titration Calorimetry (ITC):

ITC experiments were performed using MicroCal ITC_{200} microcalorimeter (Malvern, Northampton, MA)[41] in 1X PBS buffer at 25 °C with reference power 9 µcal/s. Protein and ligands were dissolved in PBS buffer. For NTD-ligands binding experiments, 20 µM purified SARS-CoV-2 NTD protein was placed into the cell and ligands in the range of 200-400 µM were filled in the syringe. After equilibration, the total 20 injections of syringe samples were titrated in the cell with one injection of 0.4 µL followed by 19 injections of 2 µL at an interval of 220 sec. The one-site binding model analysed the binding parameters to obtain ΔH, ΔS, and K_D values using Malvern's Origin 7.0 Microcal-ITC200 analysis software.

Cell culture and virus preparation:

Vero cells were cultured in Eagle's minimum essential medium (EMEM; MP Bio), supplemented with 10% Fetal Bovine Serum (FBS; Himedia), 1 µg/ml Gentamycin (Himedia). Cells were maintained and grown in a humidified atmosphere at 37 °C and 5% CO_2. SARS-CoV-2/Human/IND/CAD1339/2020 (an isolate from SARS-CoV-2 patient in India) was propagated, stored and titrated using Vero cells. Virus isolate was genetically characterized by whole genome sequencing (GenBank accession no: MZ203529) and was passaged in Vero cells. Briefly, virus stocks were prepared by adding the virus to a confluent monolayer of Vero cells for two days until cytopathic effect (CPE) was observed. The supernatant was collected and clarified by low-speed centrifugation prior to being aliquoted for storage at -80 °C. The titer of virus stock was determined as 50% tissue culture infectious dose **(**$TCID_{50}$/ml) in the confluent monolayer of Vero cells in 96-well plate. The virus titer was determined as $1X10^{6.74}$ $TCID_{50}$/mL. All studies on infectious SARS-CoV-2 were performed in Biosafety level 3 facility at Indian Veterinary Research Institute (IVRI), Izatnagar Bareilly, after obtaining necessary approvals from Biosafety Committees.

Assessment of cell viability:

MTT assay was used to assess the cytotoxic effects of compounds on Vero cells[42]. Briefly, 1×10^4 cells/well were seeded in a 96-well cell culture plate and was allowed to attach for 24 h at 37 °C and 5% CO_2. At confluency of ~80%, the media was removed from all wells, and the cells were washed with sterile PBS. Subsequently, the cells were treated with increasing concentration of compounds dissolved in 2% EMEM media for 48 h at 37 °C and 5% CO_2. Post incubation, MTT [3-(4,5-dimethylthiazol-2-yl)-2,5-diphenyl tetrazolium bromide] (0.5 mg/ml) was added to each well followed by an incubation period of 4 h at 37 °C and 5% CO_2 in dark. After incubation, the media was removed from all wells, and the blue formazan crystals were then dissolved in Dimethyl sulfoxide (DMSO, 100 uL/well). Absorbance was measured at 570 nm using a multimode plate reader. Values represent the mean, and error bars denote the standard deviation from duplicate reactions. Cell viability was calculated as a percentage against the untreated control, and the data were plotted using GraphPad prism to calculate the 50% cytotoxic concentration (CC_{50}) of identified compounds.

Assessment of the antiviral potential of compounds against NTD:

For the antiviral assay, 70-80% confluent Vero cells were incubated with various dilutions of compounds in 2% EMEM for 2 h at 37 ºC at 5% CO_2 tension. After incubation, the cells were washed with PBS and were infected with SARS-CoV-2 at 0.01 Multiplicity of infection (MOI) in media without FBS and again incubated for 2 h. The media was subsequently removed after incubation, and a fresh medium containing different concentrations of candidate compounds were added to the respective wells. The plate was incubated for 48 h for assessment of CPE. Following this, 100 µL of cell culture supernatant was harvested for viral RNA extraction using the TRU-PCR viral RNA extraction kit (BlackBio) according to the manufacturer's instructions. Quantitative real-time RTPCR (qRT-PCR) was carried out using the commercial COVISure-COVID-19 Real-Time PCR kit (Genetix) as per the manufacturer’s instructions to quantify the virus yield as described previously[43,44]. A reference drug hydroxychloroquine was used as a positive control. Percentage inhibition versus concentration graph was plotted, and half maximal effective concentration (EC_{50}) values were calculated using the non-linear regression fit model of GraphPad Prism. Data are represented as mean, and error bars corresponds to the standard deviation for a duplicate set of reactions.

Quantification of the antiviral potential of selected compounds by endpoint titration:

Antiviral potential of selected compounds was further evaluated by $TCID_{50}$/ml, and virus titers were established by Reed and Muench method[45]. For this purpose, Vero cells were seeded in a 96-well cell culture plate and were incubated at 37 ºC and 5% CO_2 tension overnight. 10-fold serial dilution of cell-culture supernatant samples (compound treated) collected 48 hours post-infection (hpi) of the antiviral assay were used to infect confluent monolayer of Vero cells in 96-well plate (50 uL/well). Untreated virus stock samples were used as positive control, and samples with only cell-culture media were used as a negative control to infect cells. The plate was incubated for 72 h at 37 ºC and 5% CO_2 and monitored for the presence and absence of CPE. Following the incubation period, the media was discarded and the cells were fixed with 10% paraformaldehyde for 6-8 h at room temperature. After fixation, the cells were stained with 0.5% crystal violet. The dilution at which 50% of cells were infected was calculated, and the data is reported as $\log_{10}$ $TCID_{50}$/ml. Titer of virus produced from compound-treated cells and control cells is presented as $TCID_{50}$/ml.

Results:

Structure-based identification of NTD inhibitors

To mediate viral RNA encapsidation, the NTD of coronavirus N-protein possess an RNA binding pocket that is basic and hydrophobic in nature. This pocket is responsible for binding to the viral RNA genome[25]. The crystal structure of NTD in complex with GMP from SARS-CoV and crystal structure of NTD in complex with PJ34 from HCoV-OC43 lead to the identification of the druggable RNA binding pocket coronaviruses[24,26,28,46]. The published data for the NTD of HCoV-OC43 N-protein indicates that the binding of small molecules in this pocket competes and hinders the binding of RNA in the pocket and thus, makes this pocket a potential antiviral therapeutic target[26,47,48]. Comparative sequence analysis of the NTD of SARS-CoV-2 N-protein with other important members of the family *coronaviridae* demonstrates that the residues of the druggable pocket are mostly conserved (Figure 1). Structural alignment of selected coronaviruses NTD structures in complex with GMP, PJ34 inhibitor, and Adenosine monophosphate (AMP) binding sites superimposition confirms the spatial conservation of the key residues involved in the binding to the RNA [Figure 1 (b-e)].

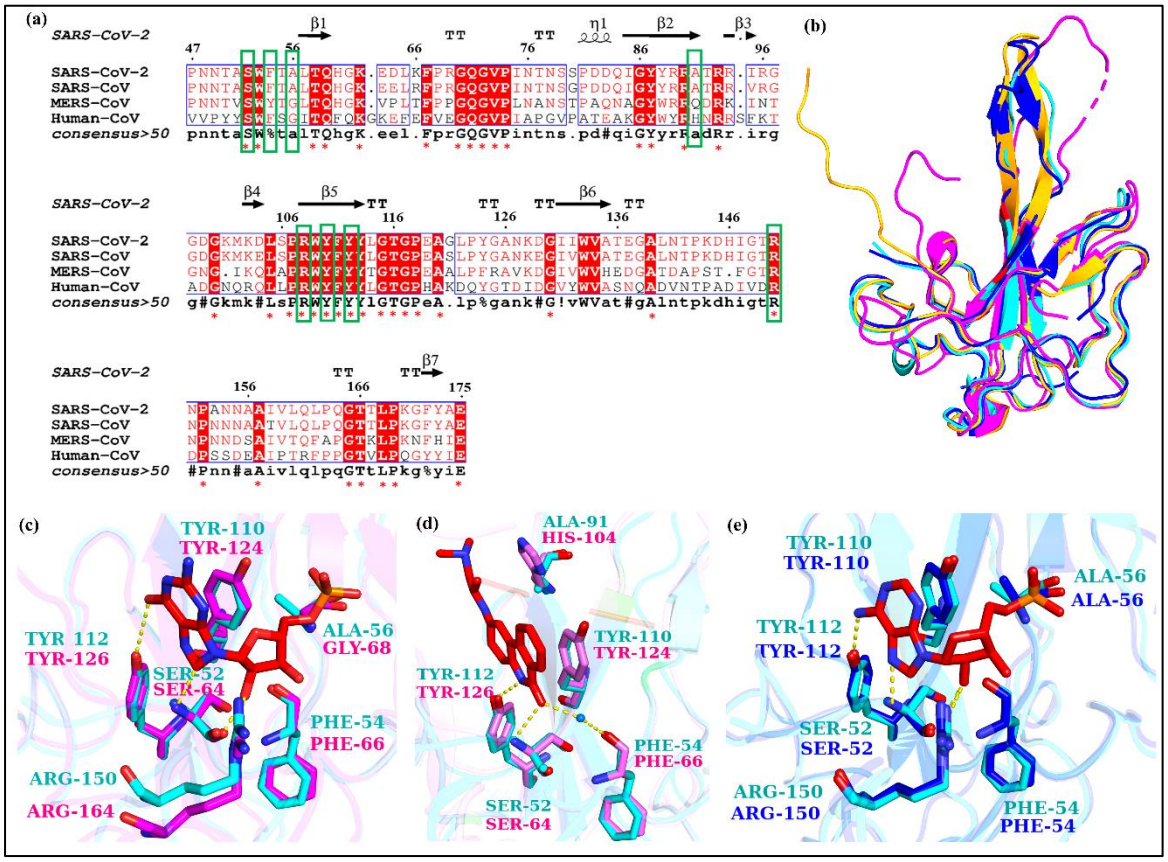

Figure 1: Sequence and structural comparison of RNA binding pockets of coronaviruses: (a) Multiple sequence alignment of SARS-CoV-2 N-NTD (PDB ID: 6M3M) with SARS-CoV N-NTD (PDB ID: 2OFZ), MERS-CoV (PDB ID: 4UD1), and HCoV-OC43 (PDB ID 4LI4). Red color stars show conserved residues, and green boxes indicate the residues present in the RNA binding site. (b) The three-dimensional structural alignments of SARS-CoV-2 (Cyan), SARS-CoV (Blue), MERS-CoV (Yellow-orange), and HCoV-OC43 (Magenta) (c) Structural superimposition of GMP binding residues of SARS-CoV-2 (PDB ID: 6M3M) and HCoV-OC43 (PDB ID: 4LM9) with GMP (Red stick). (d) Structural superimposition of GMP binding residues of SARS-CoV-2 (PDB ID: 6M3M) and HCoV-OC43 (PDB ID: 4KJX) with ligand PJ34 (Red stick). (e) Structural superimposition of AMP binding residues of SARS-CoV-2 (PDB ID: 6M3M), SARS-CoV (PDB ID: 2OFZ) with AMP (Red stick), where sticks represent the key RNA binding residues.

Based on these sequence and structural comparisons, molecular docking of GMP targeting the RNA binding residues (Ser52, Phe54, Ala56, Tyr110, Tyr112, and Arg150) of SARS-CoV-2 NTD was performed using AutoDock Vina and AutoDock Tools. Detail molecular interaction analysis using PyMol and LigPlot^{+} shows the participation of Ala56 and Tyr112 in H-bond formation with GMP and Ala51, Ser52, Thr55, Ala91, Arg108, Tyr110, and Arg150 residues were found to interact with GMP through hydrophobic interactions (Figure 2). The B.E. of the NTD-GMP complex was -5.9 kcal/mol. This B.E. of the complex was taken as reference to filter and select potential small molecules from the compound libraries through *in silico* screening. Computer-aided virtual screening of three different libraries (FDA approved library, Natural product library, and LOPAC^{1280} library) was performed to identify potential antivirals against the NTD of SARS-CoV-2 N-protein. The AutoDock Vina in PyRx 0.8 was used for performing virtual screening. These libraries were screened against the RNA binding pocket of NTD. The best-fit and high-affinity molecules from the FDA approved library (BMS-92711, Telmisartan, and Bictegravir) and the natural product library (Alisol_B, Apatinib, and Nomilin) were selected. The top six molecules from the LOPAC^{1280} library (ANA-12, Galloflavin_Potassium, BMS-189453, MCC-555, Bisdemethoxycurcumin, and Icilin) were selected after comparing the B.E. with the NTD-GMP complex. These selected twelve molecules were further subjected for molecular docking study to analyse the NTD-ligands interactions in more details.

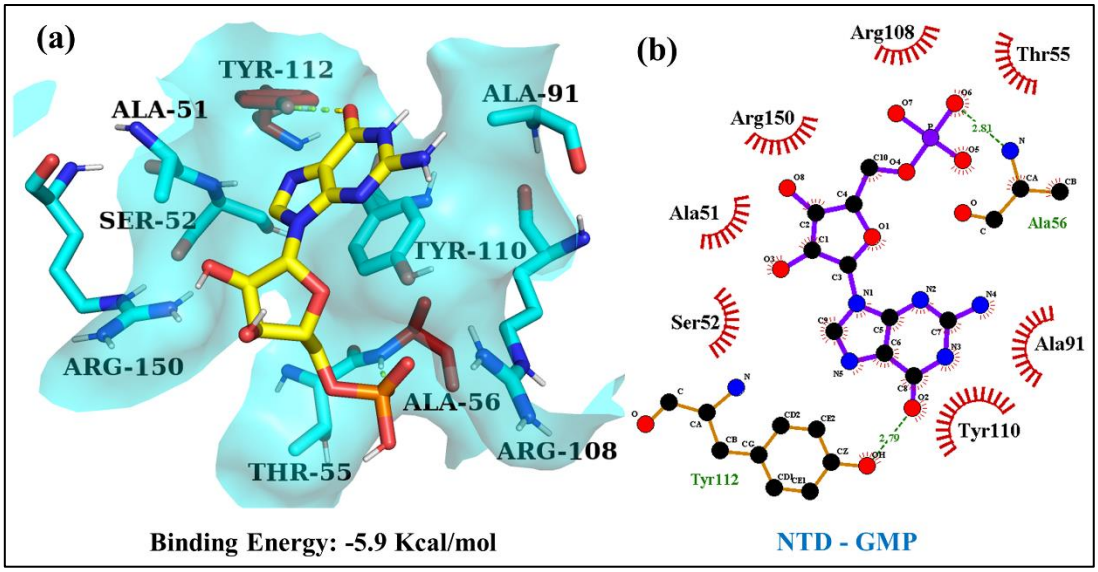

Figure 2: Detailed schematic representation of NTD-GMP complex: (a) Three-dimensional molecular docking interaction analysis of GMP with RNA binding pocket of NTD using PyMol. Sticks represent the interacting residues of the NTD-GMP complex. NTD amino acid residues are shown by red and cyan colour while GMP is shown in yellow. The surface covered by interacting residues is shown by cyan colour with 60% transparency. Red coloured residues Ala56 and Tyr112 show H-bond interactions while cyan coloured stick residues Ala51, Ser52, Thr55, Ala91, Arg108, Tyr110, and Arg150 of NTD show hydrophobic interactions with GMP. H-bond interactions are shown by yellow coloured dotted line. (b) Two-dimensional pictorial representation NTD-GMP complex using LigPlot+. GMP is represented in purple colour stick, while the residues of NTD involved in H-bond interactions are displayed as brown coloured sticks, and green coloured dotted lines show their H-bond lengths. The red stellate residues represent hydrophobic interactions.

Molecular docking study of ligands targeting the RNA binding pocket of NTD:

The selected compounds: BMS-92711, Telmisartan, Bictegravir, Alisol_B, Apatinib, Nomilin, ANA-12, Galloflavin_Potassium, BMS-189453, MCC-555, Bisdemethoxycurcumin, and Icilin were docked into the GMP binding pocket of SARS-CoV-2 NTD using AutoDock Vina and AutoDockTools. These compounds showed B.E. in the range of -6.8 to -7.9 kcal/mol, which is significantly higher than the B.E. of GMP (Table 1). Binding conformation and interactions of these selected small molecules in the RNA binding pocket of NTD show that the key residues involved in binding to GMP or RNA also participates in binding to these molecules (Figure 3 and 4). The comparative analysis of docked NTD-ligand complexes with NTD-GMP complex shows the involvement of additional residues of the RNA binding pocket that do not participate in GMP binding (Table 1).

Table 1. Molecular docking of screened compounds against the nucleotide-binding site of NTD protein provides detailed information about the values of binding energy (kcal/mol), H-bond interactions & hydrophobic interactions.

Compound	Binding Energy (kcal/mol)	H-Bond Interactions		Hydrophobic Interactions
		No. of bonds	Residues	
FDA Approved compounds				
BMS-927711	-7.9	1	Tyr110	Thr50, Ala51, Thr55, Ala56, Ala91, Arg108, Tyr112, Pro118, Arg150, Ala157
Telmisartan (MICARDIS)	-7.6	2	Ser52, Tyr112	Ala51, Thr55, Ala56, Ala91, Arg108, Tyr110, Arg150, Pro152, Ala156, Ala157
Bictegravir	-7.5	6	Ser52, Arg89, Tyr112, Arg150	Ala51, Tyr110, Pro118
Natural compounds				
Alisol_B	-7.6	2	Thr50, Arg150	Ala51, Thr55, Arg89, Ala91, Tyr110, Tyr112, Pro118, Ala157
Apatinib	-7.4	1	Arg89	Thr55, Ala56, Ala91, Arg108, Tyr110, Tyr112, Arg150, Ala157
Nomilin	-7.1	4	Ala56, Arg150, Ala157	Thr50, Thr55, Tyr110, Pro152
LOPAC compounds				
ANA-12	-7.4	2	Tyr110, Arg150	Ala51, Ser52, Phe54, Thr55, Ala56, Ala91, Arg108, Tyr112, Ala157
Galloflavin Potassium	-7.2	9	Ser52, Arg90, Arg89, Tyr112, Arg150	Ala51, Ala91, Tyr110
BMS-189453	-6.9	2	Arg89, Tyr112	Thr55, Ala56, Ala91, Tyr110, Arg150, Asn151, Pro152, Ala157
MCC-555	-6.9	3	Arg89, Tyr112, Arg150	Ser52, Thr55, Ala56, Ala91, Tyr110, Pro118

Bisdemethoxycurcumin	-6.8	3	Arg89, Arg150	Ala51, Ser52, Thr55, Ala56, Arg108, Tyr110, Tyr112, Pro118, Ala174
Icilin	-6.8	3	Arg89, Tyr112, Arg150	Thr50, Ala51, Ser52, Thr55, Ala91, Tyr110, Ala157

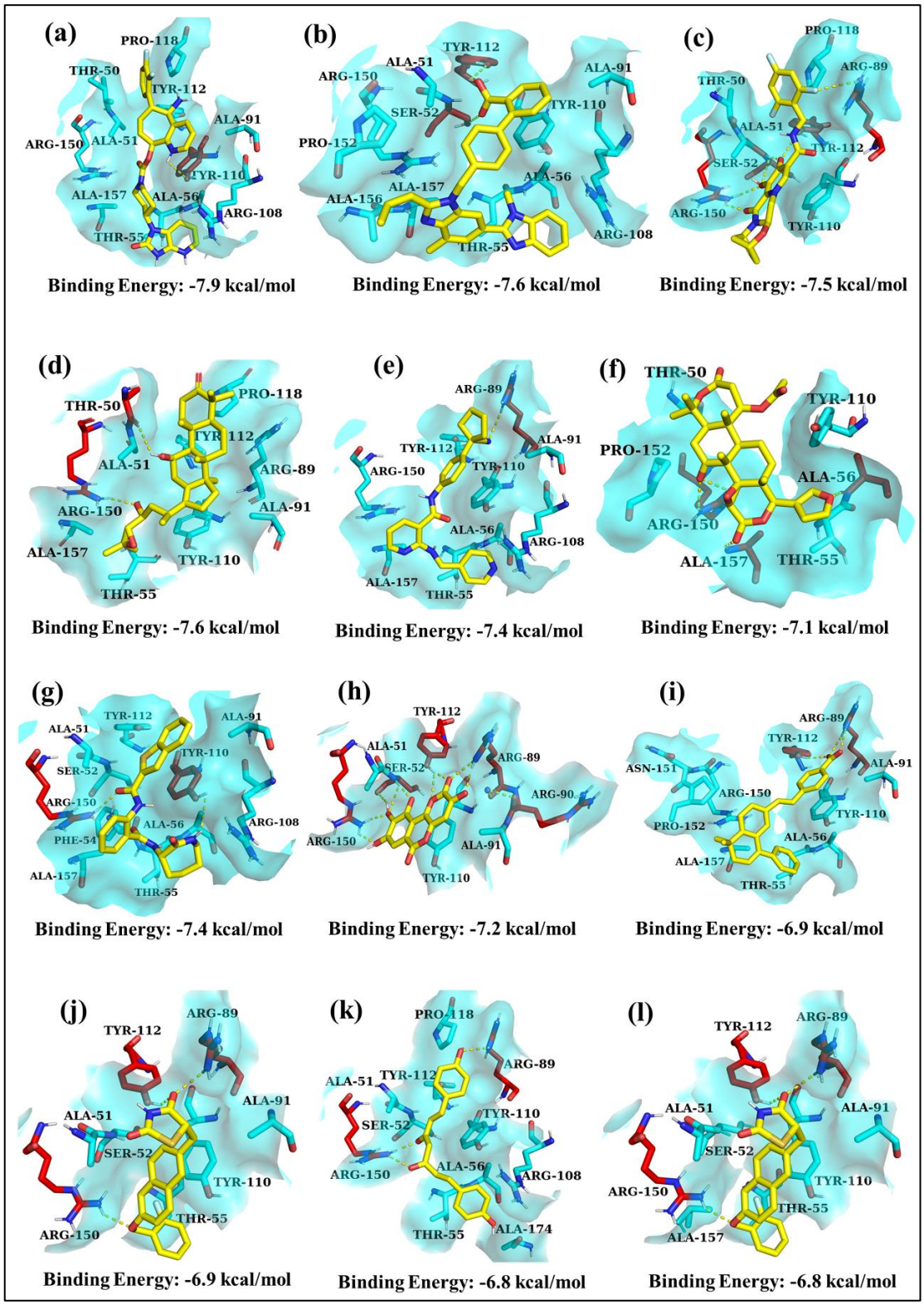

Figure 3: The interaction analysis of best fit binding conformation inferred from molecular docking of top hit compounds against the 3D structure of NTD. (a) BMS-927711, (b) Telmisartan (MICARDIS), (c) Bictegravir, (d) Alisol_B, (e) Apatinib, (f) Nomilin, (g) ANA-12 , (h) Galloflavin_Potassium, (i) BMS-189453 , (j) MCC-555, (k) Bisdemethoxycurcumin, and (l) Icilin occupy the RNA binding site in the similar manner as that of GMP. Ligands are shown in yellow coloured sticks, whereas the interacting residues of NTD are represented by cyan and red coloured sticks. The surface covered by interacting residues is shown by cyan colour with 60% transparency. The residues involved in H-bond interactions are shown in red coloured sticks and residues involved in hydrophobic interactions are involved in cyan coloured sticks. Yellow coloured dotted lines show the intermolecular H-bond interactions.

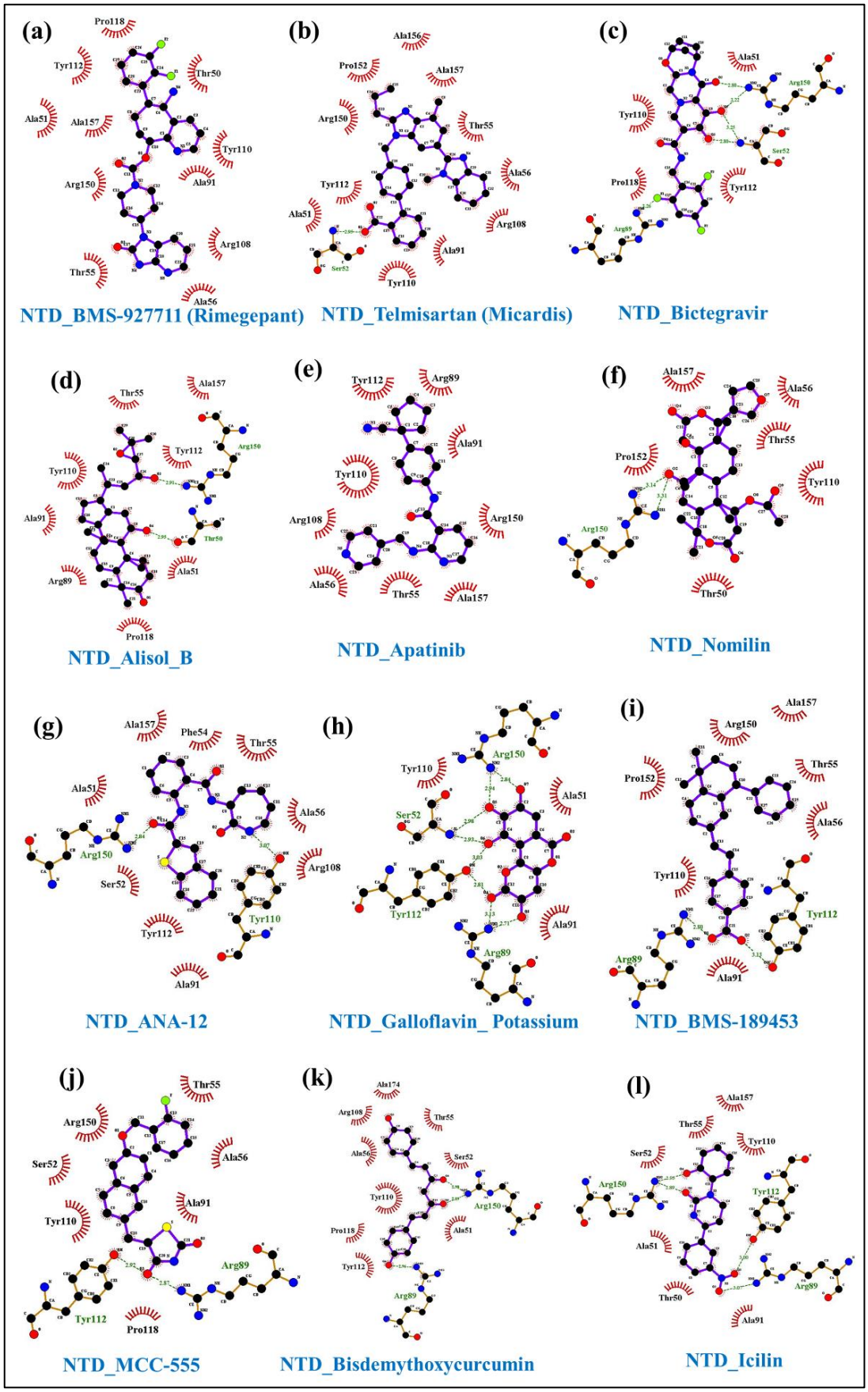

Figure 4: Illustrative two-dimensional pictorial representations of NTD-ligands interactions using LigPlot+. Ligands (a) BMS-927711, (b) Telmisartan, (c) Bictegravir, (d) Alisol_B, (e) Apatinib, (f) Nomilin, (g)

ANA-12 , (h) Galloflavin_Potassium, (i) BMS-189453 , (j) MCC-555, (k) Bisdemethoxycurcumin, and (l) Icilin are represented in purple coloured sticks. The residues of NTD involved in hydrophobic interactions are represented with semi-circled red colour, brown colour sticks represent residues involved in intermolecular H-bond interactions, and green coloured dotted lines show their bond lengths.

The detailed analysis of H-bonds and hydrophobic interactions were performed using PyMol and LigPlot^{+} showed that residues Ala51, Ser52, Thr55, Phe54, Ala56, Thr58, Ala91, Arg108, Tyr110, Tyr112, Arg150, Ala157, and Ala174 are key interacting residues (Figure 3, 4 and Table 1). The additional residues (underlined in Table 1) which are participating in the binding of selected molecules and not present in the NTD-GMP complex seems to favour and increase the B.E. of NTD-ligand complexes. FDA approved compounds BMS-927711 interacts with one H-bond (Tyr110), telmisartan interacts with NTD by forming two H-bonds (Ser52 and Tyr112), and Bictegravir shows six H-bonds with four residues Ser52, Arg89, Tyr112, and Arg150. Natural product compounds Alisol_B interacts with two H-bonds (Thr50 and Arg150), Apatinib with one H-bond (Arg89), and Nomilin displays four H-bonds with residue Ala56, Arg150, and Ala157. LOPAC^{1280} compounds ANA-12 interacts with two H-bonds (Tyr110 and Arg150), Galloflavin_Potassium forms nine H-bonds with residues Ser52, Arg89, Arg90, Try112, and Arg150, BMS-189453 with two H-bonds (Arg89 and Tyr112), MCC-555, and Icilin form three H-bonds with residues Arg89, Tyr112, and Arg150, and Bisdemethoxycurcumin forms three H-bonds with residues Arg89 and Arg150 (Figure 3, 4 and Table 1). Further, the binding of these selected small molecules has been validated using the purified NTD SARS-CoV-2 protein (Figure SF1) by ITC experiments.

Thermodynamic binding analysis of inhibitors to NTD:

To determine the binding of selected compounds BMS-92711, Telmisartan, Bictegravir, Alisol_B, Apatinib, Nomilin, ANA-12, Galloflavin_Potassium, BMS-189453, MCC-555, Bisdemethoxycurcumin, and Icilin to the target protein, the thermodynamic binding titration experiments were performed using MicroCal ITC$_{200}$ microcalorimeter (Malvern, Northampton, MA) at 25 °C. The compounds and protein were diluted in 1XPBS buffer at pH 7.3. Ten compounds except Galloflavin_Potassium were titrated at a concentration of 200 μM (in syringe) against 20 μM NTD (in cell) whereas Galloflavin_Potassium was titrated at a concentration of 400 μM by keeping all other parameters same. The compound Alisol_B was not determined because of unavailability in India. ITC isotherms were jointly fit using a one site binding model for non-linear curve to determine the thermodynamic parameters such as n, K_D, ΔH, and ΔS. The data were analysed using commercially available Origin7.0 associated with Microcal-ITC200 analysis Software. ITC analysis yielded excellent equilibrium dissociation constant, K_D values such as 13 μM, 44.2 μM, 22 μM, 21.7 μM, 90 μM, 40.4 μM, 36 μM, 39.2 μM, 27.4 μM, 82.6 μM, and 26 μM for BMS-92711, Telmisartan, Bictegravir, Alisol_B, Apatinib, Nomilin, ANA-12, Galloflavin_Potassium, BMS-189453, MCC-555, Bisdemethoxycurcumin, and Icilin, respectively (Figure 5 and Table 2).

Table 2: The thermodynamic analysis of top hit compounds with NTD protein as obtained from ITC.

Protein	Ligand	n	K_D (μM)	K_A(M^{-1})	ΔH(cal/mol)	ΔS(cal/mol/degree)

NTD	BMS-927711 (Rimgepant)	1	13	$(7.65\pm1.14)10^4$	$(-17.70\pm1.871)10^4$	-571
NTD	Telmisartan (MICARDIS)	1	44.20	$(2.26)10^4\pm561$	$(-2.549)10^5\pm3787$	-835
NTD	Bictegravir	1	22	$(4.52)10^4\pm(3.64)10^3$	$(-6.567)10^4\pm2483$	-199
NTD	Alisol_B	Not determined (unavailability of the compound in India)				
NTD	Apatinib	1	21.69	$(4.61\pm1.20)10^4$	$(-2.166)10^4\pm1977$	-51.3
NTD	Nomilin	1	90	$(1.11)10^4\pm312$	$(-1.379)10^5\pm2796$	-444
NTD	ANA-12	1	40.40	$(2.47)10^4\pm712$	$(-1.819)10^5\pm3054$	-590
NTD	Galloflavin_Potassium	1	36	$(2.72)10^4\pm(1.67)10^3$	$(-2.010)10^5\pm6238$	-654
NTD	BMS-189453	1	39.21	$(2.55)10^4\pm711$	$(-4.090)10^5\pm6604$	$(-1.35)10^3$
NTD	MCC-555	1	27.4	$(3.65)10^4\pm(1.06)10^3$	$(-3.024)10^5\pm4464$	-993
NTD	Bisdemethoxycurcumin	1	82.6	$(1.21)10^4\pm384$	$(-1.632)10^5\pm3675$	-529
NTD	Icilin	1	26	$(3.83)10^4\pm(5.70)10^3$	$(-45.66\pm3.300)10^4$	$(-1.51)10^3$

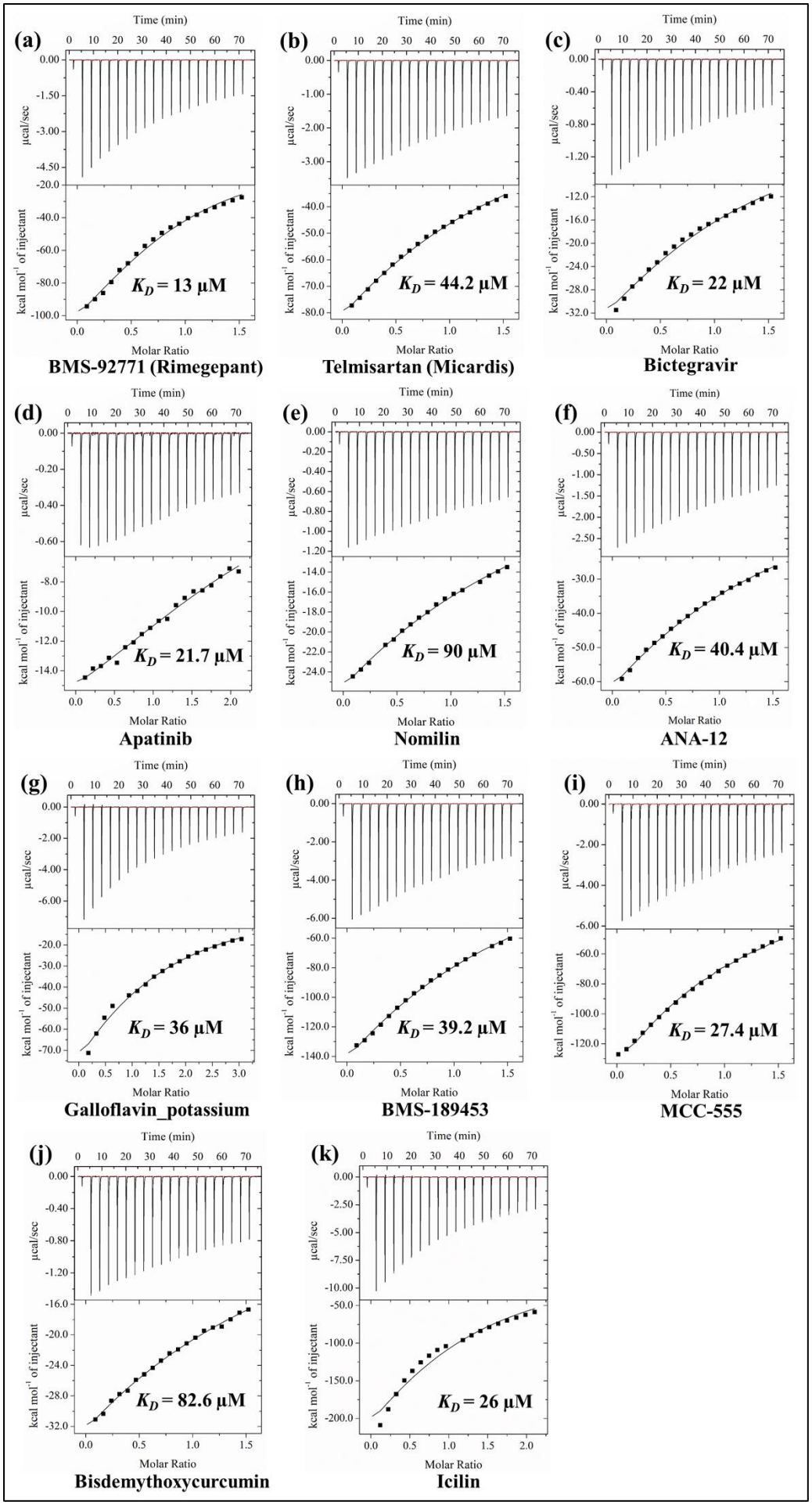
(a)
Time (min)
μcal/sec
kcal mol⁻¹ of injectant
Molar Ratio
K_D = 13 μM
BMS-92771 (Rimegepant)
(b)
K_D = 44.2 μM
Telmisartan (Micardis)
(c)
K_D = 22 μM
Bictegravir
(d)
K_D = 21.7 μM
Apatinib
(e)
K_D = 90 μM
Nomilin
(f)
K_D = 40.4 μM
ANA-12
(g)
K_D = 36 μM
Galloflavin_potassium
(h)
K_D = 39.2 μM
BMS-189453
(i)
K_D = 27.4 μM
MCC-555
(j)
K_D = 82.6 μM
Bisdemythoxycurcumin
(k)
K_D = 26 μM
Icilin

Figure 5: Binding isotherms of identified compounds using ITC: Thermodynamic profiles of ligands (a) BMS-92711, (b) Telmisartan, (c) Bictegravir, (d) Apatinib, (e) Nomilin, (f) ANA-12, (g) Galloflavin_Potassium, (h) BMS-189453, (i) MCC-555, (j) Bisdemethoxycurcumin, and (k) Icilin against the purified SARS-CoV-2 NTD protein.

Characterization of anti-SARS-CoV-2 activity of identified compounds:

Cell viability studies of the selected compounds were carried out on Vero cells using MTT assay before performing the antiviral assay to determine the CC_{50} value of the compounds. CC_{50} value is defined as the drug concentration required to reduce cell viability by 50%. CC_{50} values for all compounds are shown in Figure 6. DMSO was used as a vehicle control, and a statistically significant increase in cell cytotoxicity was observed when Vero cells were treated with increased concentrations of compounds. To assess the antiviral potential of selected compounds, Vero cells were treated with different concentrations of compounds before and after infection with SARS-CoV-2 (SARS-CoV-2/Human/IND/CAD1339/2020) at an MOI of 0.01. Cell culture supernatants were harvested at 48 hpi, and the antiviral efficacies of the selected compounds were evaluated by quantifying viral RNA in the cell culture supernatant using qRT-PCR. Among the eleven drugs that were evaluated in the present study, nine compounds displayed potential antiviral activities against SARS-CoV-2. EC_{50} of these compounds were determined using GraphPad Prism software. The EC_{50} values for the compounds MCC 555 (4.26 ±0.010 µM), Bictegravir (8.11 ± 0.014 µM), ANA-12 (4.51 ±0.002 µM), Bisdemethoxycurcumin (1.64 ± 0.003 µM), Galloflavin_Potassium (4.89 ± 0.011 µM), Icilin (4.81 ± 0.016 µM), Telmisartan (Micardis) (1.02 ± 0.594 µM), BMS-189453 (0.98 ± 0.0007 µM), and Nomilin (12.50 ± 0.156 µM) were determined (Figure 6). As elucidated from the qRT-PCR assay, treatment with the aforementioned compounds potently inhibited SARS-CoV-2 at a low micromolar range (Figure 6). Apatinib and BMS 927711 were found to be the least effective at non-toxic concentrations, and the higher doses of these compounds were observed to be highly toxic. Interestingly, a recent report also corroborates our finding of Telmisartan(Micardis), an Angiotensin II type 1 (AT1) receptor antagonist, as a potential and effective antiviral drug against treatment of SARS-CoV-2[49]. A strong inhibition pattern was observed for MCC 555, Bictegravir, ANA-12, and Bisdemethoxycurcumin with a percentage inhibition of more than 90% at low concentrations and high concentrations of these compounds was able to completely suppress SARS-CoV-2 infection. To further confirm the antiviral efficacy of these four compounds on SARS-CoV-2, cell culture supernatants harvested from antiviral assays of these compounds were further subjected to end-point assay for $TCID_{50}$ determination.

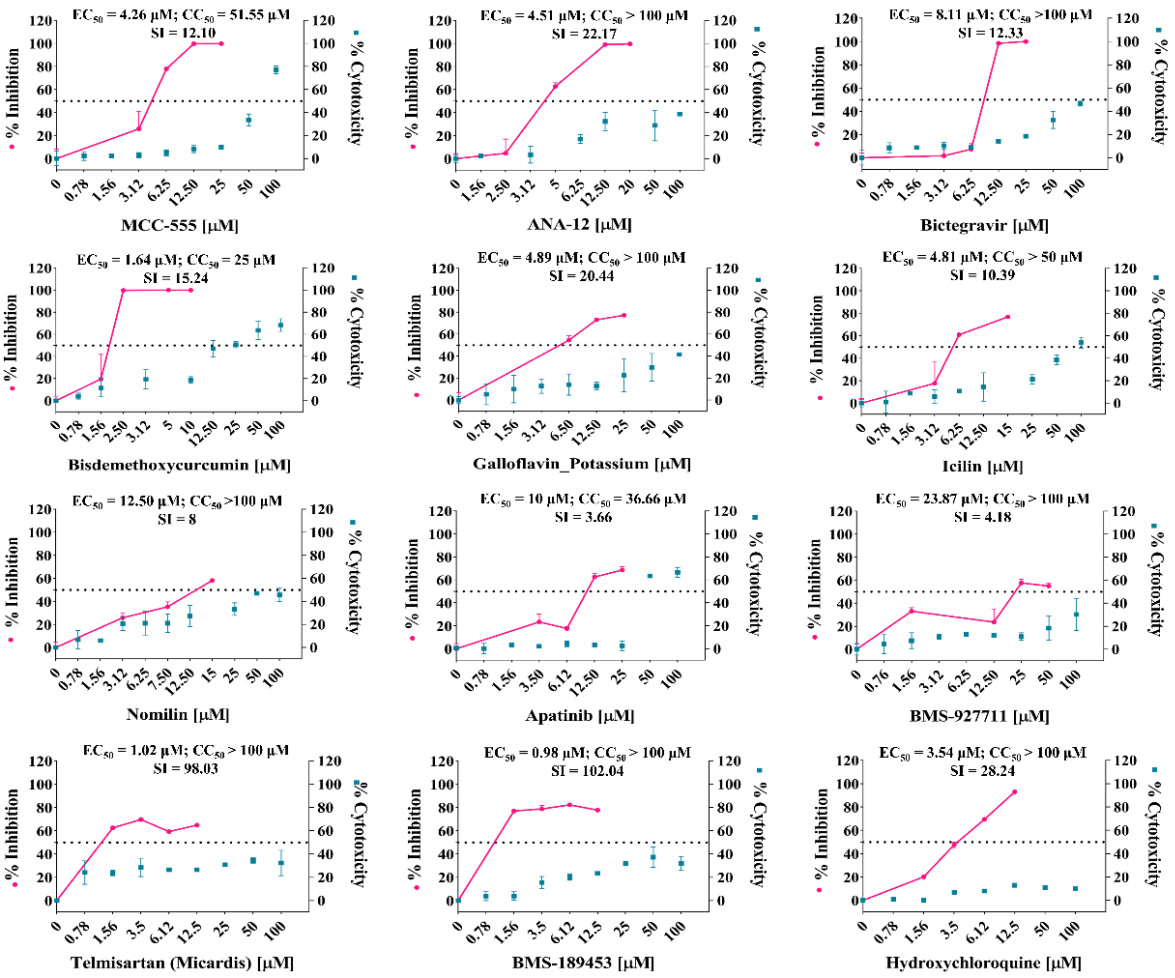

Figure 6: Anti-SARS-CoV-2 profiles of selected compounds: Vero cells were treated with different doses of compounds chosen before and after infection with SARS-CoV-2 (MOI 0.01). The viral yield in the presence and absence of compounds was quantified by qRT-PCR, and the percentage inhibition versus concentration graph was plotted. Results are representative of n = 2 and are shown as mean ± standard deviation. Cytotoxicity of these compounds was assessed using an MTT assay. The pink circles and lines specify the percentage inhibition of SARS-CoV-2 on treatment with selected compounds, and blue squares denote percentage cytotoxicity values at 48 hpi. The left and right Y-axis corresponds to percent inhibition and percentage cytotoxicity, respectively. The 50% cytotoxic concentration (CC_{50}), half maximal effective concentration (EC_{50}), and Selectivity Index (SI) values of each compound were calculated and displayed on each corresponding graph's upper panel. Values are mean and error bars are standard deviations from duplicate reactions. The data were normalized and CC_{50} and EC_{50} values were calculated using Graph Pad prism's non-linear regression fit model.

In concordance with the antiviral assay, the compound treated groups showed a significant decrease in viral titer in $TCID_{50}$ assay than those of untreated virus control at non-toxic levels. The $TCID_{50}$/ml value observed for compound treated groups was $10^{2.49}$ for MCC 555 at 25 µM, $10^{1.8}$ for Bictegravir at 25 µM, $10^{2.03}$ for Bisdemethoxycurcumin at 10 µM, and $10^{2.16}$ for ANA-12 at 20 µM in comparison to virus control group ($10^{4.34}$ $TCID_{50}$/ml). The results obtained from the $TCID_{50}$ assay displayed a dose-dependent inhibitory pattern of these four compounds against SARS-CoV-2. Taken together, these findings reveal the anti-SARS-CoV-2 activity of the nine compounds, predominantly by MCC 555, Bictegravir, ANA-12, and Bisdemethoxycurcumin.

Discussion:

In the present study, the *in silico* structure-based identification, biophysical validations and antiviral data of SARS-CoV-2 NTD demonstrates that N-protein is a promising drug target for therapeutic interventions against COVID-19. N-protein is a major structural component of the virion that plays a crucial role in viral assembly, viral genome packaging, replication, transcription, and host immune response regulation. It plays a key role in binding to the viral RNA genome by forming an RNP complex responsible for maintaining an ordered RNA conformation[50]. Furthermore, it consists of two functional domains, the encapsidation domain NTD primarily responsible for RNA-binding and the oligomerization domain CTD, separated by a disordered linker region. Previous structural studies on NTD suggest that it is highly conserved and shares structural similarities with the other coronaviruses. Revisiting previous studies for coronaviruses indicate that small molecules targeting the RNA-binding pocket of NTD hinder the interaction of N-protein with viral RNA and potentially suppress the virus replication[26].

The binding affinity and interactions of NTD-GMP complex and NTD-PJ34 complex were taken as reference to screen the molecules against RNA binding site from three selected drug libraries (Figure 1 and 2). Using a combined approach of high-throughput virtual screening and molecular docking, small molecules targeted against the RNA binding pocket of NTD were identified from the compound libraries. Three molecules from FDA approved drug library (BMS927711, Telmisartan, and Bictegravir), three compounds from the Natural compound library (Alisol_B, Apatinib, and Nomilin). Six compounds from the LOPAC library (ANA-12, Galloflavin_Potassium, BMS-189453, MCC-555, Bisdemethoxycurcumin, and Icilin) were observed to display a good docking score with high binding affinities in comparison to that of the GMP-NTD complex (Figure 3 and 4). The molecular docking results indicate that the molecules occupy the same RNA binding pocket. PyMol and LigPlot^{+} analysis reveal that the identified molecules also interact with key NTD-GMP complex residues and additional residues such as Thr50, Arg89, Arg90, Pro118, Asn151, Ala157, and Ala174. These additional interactions possibly enhance the binding affinity of the ligand towards the RNA binding pocket of NTD (Figure 3, 4, and Table1).

Further, the binding of identified molecules to the target was validated using ITC. ITC measurements were carried out to determine the thermodynamic parameters such as reaction stoichiometry (n), binding constant (K_D), enthalpy (ΔH), and entropy (ΔS). In concordance with docking studies, ITC results confirmed that the identified ligands showed high binding affinities towards NTD, with their K_D values in the lower micromolar range. The titration curves suggest that K_D values of BMS-927711, Telmisartan (Micardis), Bictegravir, Apatinib, Nomilin, ANA-12, Galloflavin_Potassium, BMS-189453, MCC-555, Bisdemythoxycurcumin, and Icilin are 13 μM, 44.2 μM, 22 μM, 21.7 μM, 90 μM, 40.4 μM, 36 μM, 39.2 μM, 27.4 μM, 82.6 μM, and 26 μM respectively (Figure 5 and Table 2). The binding constants of these ligands encouraged us to check their antiviral efficacy using cell culture-based antiviral testing. To further support the results of docking and biophysical studies, the antiviral potential of the selected eleven molecules were assessed using cell-based *in vitro* assays. qRT–PCR and $TCID_{50}$/ml studies demonstrated that MCC555, Bictegravir, ANA-12, and Bisdemethoxycurcumin were observed to display strong antiviral effects against SARS-CoV-2, with EC_{50} values of 4.26 ±0.010 μM, 8.11 ± 0.014 μM, 4.51 ±0.002 μM, and 1.64 ± 0.003

µM, respectively (Figure 6). Apatinib and BMS927711 were observed to be least effective at non-toxic concentrations.

These selected compounds are reported as anticancerous, anti-diabetic, and some are commercially available as antivirals (Table 3). Bictegravir and Galloflavin are reported HIV-1 integrase inhibitors[51–55]. Telmisartan is an FDA approved drug that acts as an antagonist of the angiotensin-II receptor[56]. These angiotensin receptor blockers (ARBs) can aid in reducing COVID-19-related inflammatory responses, which would otherwise lead to acute respiratory distress syndrome (ARDS)[56,57]. BMS 189453 is a potent Retinoic acid Receptor (RAR) antagonist. Published reports suggest that inhibition of RAR suppresses the production of cytokine IL-17 by blocking differentiation of T-helper cells-2, eventually reducing inflammatory effects on lungs[58,59]. Several glucose-lowering agents, such as metformin or insulin, are the most prescribed drugs for managing blood glucose levels in SARS-CoV-2 infected patients. Interestingly, another anti-diabetic drug MCC-555 reported to sensitize insulin signalling, can aid in the proper management of blood glucose levels, and amend inflammatory responses during SARS-CoV-2 infections[60,61]. Bisdemethoxycurcumin, a naturally occurring curcumin analogue, and Icilin, an activator of Transient Receptor Potential Melastatin–8 (TRPM8), are reported to possess anti-inflammatory properties and may also attenuate systemic inflammation or lung injury[62,63]. The inhibitory potential of the identified compounds and their reported clinical and pharmacological profile indicates that repurposing these drugs as monotherapy or combination therapy, should substantially speedup the drug development process against COVID-19 (Table 3).

With the frequent emergence of highly transmissible and immune escape variants of SARS-CoV-2, concern grows over the effects of these mutations on the efficacy of currently deployed vaccines and therapeutic drugs. Notably, the presently circulating SARS-CoV-2 variants of concern (VOCs), Omicron and Delta, carry several N-protein mutations with only D63G substitution in the N-NTD of Delta variant[20]. While only the D63G mutation resides in the N-NTD of the delta variant, the mutation is not a part of the highly conserved GMP binding pocket of N-protein[50]. Based on these observations, it can be inferred that the molecules identified in this study will presumably act on emerging variants as well.

In summary, the findings of the combined structure-assisted computational, biophysical and *in vitro* antiviral approaches of this study first time unravels effective anti-SARS-CoV-2 molecules that target the RNA binding pocket of N-protein NTD. The identified new compounds are highly potent in impeding the SARS-CoV-2 virus replication with EC_{50} in the range of 0.98 µM-10 µM. To develop antiviral therapy using these, further studies to verify the efficacy of these molecules, using relevant mouse models *in vivo* studies are needed to take these molecules for human clinical trials.

Table 3: Two-dimensional chemical structure of identified compounds and their reported pharmacological functions.

S. No	Compound Name	Structure	Disease	Function
1.	BMS-927711 (Rimgepant)	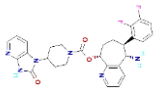	Preventive treatment of migraine	Antagonist of the CGRP receptor[64,65,66]

2.	Telmisartan (MICARDIS)	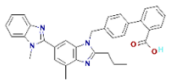	Treatment of hypertension	Angiotensin II type 1 (AT1) receptor antagonist used in the management of hypertension.[67,68]
3.	Bictegravir	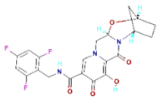	Treatment of HIV infection	Antiviral drug[51,52]
4.	Apatinib	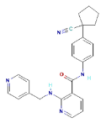	Treatment of cancer (Breast cancer, lung cancer)	Antineoplastic Agents, Protein Kinase Inhibitors[69]
5.	Nomilin	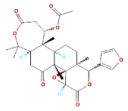	Inhibition of tumor progression by naturally occurring terpenoids	Triterpenoid present in common edible citrus fruits with putative anticancer properties.[70]
6.	ANA-12	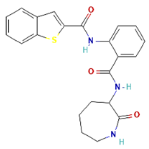	Anti-depressant	Dopamine D3 receptor[71,72,73]
7.	Galloflavin_Potassium	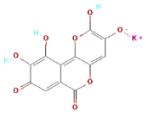	HIV-1 integrase inhibitors	Antiviral against HIV-1 and a Lactate dehydrogenase inhibitor[53,54,55]
8.	BMS-189453	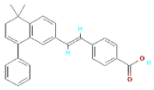	Treatment of arthritis	Synthetic retinoid receptor antagonist[74]
9.	MCC-555	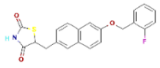	Anti-proliferative, Anti-diabetic	Peroxisome proliferator-activated receptor ligand[75,76]
10.	Bisdemethoxycurcumin	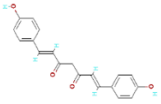	Anti-inflammatory, Anti-diabetic	Antioxidant[77,78]

11.	Icilin	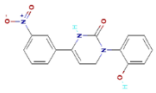	Cooling agent, Treatment of diseases digestive system	Calcium Channel Agonists[79,80,81]

References:

1. Andersen, K. G., Rambaut, A., Lipkin, W. I., Holmes, E. C. & Garry, R. F. The proximal origin of SARS-CoV-2. *Nat. Med. 2020 264* **26**, 450–452 (2020).
2. Naqvi, A. A. T. *et al.* Insights into SARS-CoV-2 genome, structure, evolution, pathogenesis and therapies: Structural genomics approach. *Biochim. Biophys. Acta - Mol. Basis Dis.* **1866**, 165878 (2020).
3. Wu, A. *et al.* Genome Composition and Divergence of the Novel Coronavirus (2019-nCoV) Originating in China. *Cell Host Microbe* **27**, 325–328 (2020).
4. 500. https://www.who.int/csr/don/12-january-2020-novel-coronavirus-china/en/.
5. COVID Live Update: 223,441,479 Cases and 4,610,403 Deaths from the Coronavirus - Worldometer. https://www.worldometers.info/coronavirus/.
6. Ortiz-Prado, E. *et al.* Clinical, molecular, and epidemiological characterization of the SARS-CoV-2 virus and the Coronavirus Disease 2019 (COVID-19), a comprehensive literature review. *Diagn. Microbiol. Infect. Dis.* **98**, 115094 (2020).
7. Masters, P. S. The Molecular Biology of Coronaviruses. *Adv. Virus Res.* **66**, 193–292 (2006).
8. Pyrc K, Berkhout B, van der H. L. The novel human coronaviruses NL63 and HKU1. *J. Virol.* **81**, 3051–3057 (2007).
9. Gordon, D. E. *et al.* A SARS-CoV-2 protein interaction map reveals targets for drug repurposing. *Nat. 2020 5837816* **583**, 459–468 (2020).
10. Fang SG, Shen H, Wang J, Tay FP, L. D. Proteolytic processing of polyproteins 1a and 1ab between non-structural proteins 10 and 11/12 of Coronavirus infectious bronchitis virus is dispensable for viral replication in cultured cells. *Virology* **379**, 175–180 (2008).
11. EJ, S. *et al.* Unique and conserved features of genome and proteome of SARS-coronavirus, an early split-off from the coronavirus group 2 lineage. *J. Mol. Biol.* **331**, 991–1004 (2003).
12. V, T. *et al.* Mechanisms and enzymes involved in SARS coronavirus genome expression. *J. Gen. Virol.* **84**, 2305–2315 (2003).
13. McBride, R., Zyl, M. van & Fielding, B. C. The Coronavirus Nucleocapsid Is a Multifunctional Protein. *Viruses* **6**, 2991 (2014).
14. Garoff, H., Frischauf, A. M., Simons, K., Lehrach, H. & Delius, H. The capsid protein of Semliki Forest virus has clusters of basic amino acids and prolines in its amino-

terminal region. *Proc. Natl. Acad. Sci. U. S. A.* **77**, 6376–6380 (1980).
15. Garoff, H., Sjöberg, M. & Cheng, R. H. Budding of alphaviruses. *Virus Res.* **106**, 103–116 (2004).
16. Fatma, B. *et al.* Alphavirus capsid protease inhibitors as potential antiviral agents for Chikungunya infection. *Antiviral Res.* **179**, 104808 (2020).
17. CK, C. *et al.* Multiple nucleic acid binding sites and intrinsic disorder of severe acute respiratory syndrome coronavirus nucleocapsid protein: implications for ribonucleocapsid protein packaging. *J. Virol.* **83**, 2255–2264 (2009).
18. Fan, H. *et al.* The Nucleocapsid Protein of Coronavirus Infectious Bronchitis Virus: Crystal Structure of Its N-Terminal Domain and Multimerization Properties. *Structure* **13**, 1859 (2005).
19. Hurst, K. R., Koetzner, C. A. & Masters, P. S. Identification of In Vivo-Interacting Domains of the Murine Coronavirus Nucleocapsid Protein. *J. Virol.* **83**, 7221–7234 (2009).
20. Lu, S. *et al.* The SARS-CoV-2 nucleocapsid phosphoprotein forms mutually exclusive condensates with RNA and the membrane-associated M protein. *Nat. Commun. 2021 121* **12**, 1–15 (2021).
21. Peng TY, Lee KR, T. W. Phosphorylation of the arginine/serine dipeptide-rich motif of the severe acute respiratory syndrome coronavirus nucleocapsid protein modulates its multimerization, translation inhibitory activity and cellular localization. *FEBS J.* **275**, 4152–4163 (2008).
22. Grossoehme, N. E. *et al.* Coronavirus N Protein N-Terminal Domain (NTD) Specifically Binds the Transcriptional Regulatory Sequence (TRS) and Melts TRS-cTRS RNA Duplexes. *J. Mol. Biol.* **394**, 544–557 (2009).
23. H, F. *et al.* The nucleocapsid protein of coronavirus infectious bronchitis virus: crystal structure of its N-terminal domain and multimerization properties. *Structure* **13**, 1859–1868 (2005).
24. Papageorgiou, N. *et al.* Structural characterization of the N-terminal part of the MERS-CoV nucleocapsid by X-ray diffraction and small-angle X-ray scattering. *urn:issn:2059-7983* **72**, 192–202 (2016).
25. Kang, S. *et al.* Crystal structure of SARS-CoV-2 nucleocapsid protein RNA binding domain reveals potential unique drug targeting sites. *Acta Pharm. Sin. B* **10**, 1228–1238 (2020).
26. Lin, S. Y. *et al.* Structural basis for the identification of the N-terminal domain of coronavirus nucleocapsid protein as an antiviral target. *J. Med. Chem.* **57**, 2247–2257 (2014).
27. Dinesh, D. C. *et al.* Structural basis of RNA recognition by the SARS-CoV-2 nucleocapsid phosphoprotein. *PLoS Pathog.* **16**, (2020).
28. Saikatendu, K. S. *et al.* Ribonucleocapsid Formation of Severe Acute Respiratory Syndrome Coronavirus through Molecular Action of the N-Terminal Domain of N Protein. *J. Virol.* **81**, 3913–3921 (2007).
29. Dhankhar, P., Dalal, V., Singh, V., Tomar, S. & Kumar, P. Computational guided identification of novel potent inhibitors of N-terminal domain of nucleocapsid protein of severe acute respiratory syndrome coronavirus 2. *https://doi.org/10.1080/07391102.2020.1852968* (2020) doi:10.1080/07391102.2020.1852968.
30. Montes-Grajales, D. *et al.* In silico drug repurposing for the identification of potential candidate molecules against arboviruses infection. *Antiviral Res.* **173**, 104668 (2020).
31. Mercorelli, B., Palù, G. & Loregian, A. Drug Repurposing for Viral Infectious Diseases: How Far Are We? *Trends Microbiol.* **26**, 865–876 (2018).

32. Caithness Biotechnologies - Focussed libraries for drug discovery. http://www.caithnessbiotechnologies.com/products.html.
33. LOPAC®1280. https://www.sigmaaldrich.com/IN/en/product/sigma/lo1280?gclid=Cj0KCQjw4eaJBhDMARIsANhrQAB1IuHF4JTei1ME1uaJQk5Pc024Y4gEsBbXwVKwbzVq2RVH8NgPcnAaAg-QEALw_wcB.
34. Robert, X. & Gouet, P. Deciphering key features in protein structures with the new ENDscript server. *Nucleic Acids Res.* **42**, W320–W324 (2014).
35. Corpet, F. Multiple sequence alignment with hierarchical clustering. *Nucleic Acids Res.* **16**, 10881 (1988).
36. Delano, W. L. PyMOL: An Open-Source Molecular Graphics Tool.
37. Morris, G. M. *et al.* AutoDock4 and AutoDockTools4: Automated Docking with Selective Receptor Flexibility. *J. Comput. Chem.* **30**, 2785 (2009).
38. Trott, O. & Olson, A. J. AutoDock Vina: improving the speed and accuracy of docking with a new scoring function, efficient optimization and multithreading. *J. Comput. Chem.* **31**, 455 (2010).
39. Laskowski, R. A. & Swindells, M. B. LigPlot+: multiple ligand-protein interaction diagrams for drug discovery. *J. Chem. Inf. Model.* **51**, 2778–2786 (2011).
40. Dallakyan, S. & Olson, A. J. Small-molecule library screening by docking with PyRx. *Methods Mol. Biol.* **1263**, 243–250 (2015).
41. MicroCal iTC200 isothermal titration calorimeter from Malvern | Product support | Malvern Panalytical. https://www.malvernpanalytical.com/en/support/product-support/microcal-range/microcal-itc-range/microcal-itc200.
42. Moghaddam, E. *et al.* Baicalin, a metabolite of baicalein with antiviral activity against dengue virus. *Sci. Rep.* **4**, (2014).
43. Cao, R. *et al.* Anti-SARS-CoV-2 potential of artemisinins in vitro. *ACS Infect. Dis.* **6**, 2524–2531 (2020).
44. Wang, M. *et al.* Remdesivir and chloroquine effectively inhibit the recently emerged novel coronavirus (2019-nCoV) in vitro. *Cell Res. 2020 303* **30**, 269–271 (2020).
45. Reed, L. J. & Muench, H. A simple method of estimating fifty per cent endpoints. *Am. J. Epidemiol.* **27**, 493–497 (1938).
46. Peng, Y. *et al.* Structures of the SARS-CoV-2 nucleocapsid and their perspectives for drug design. *EMBO J.* **39**, e105938 (2020).
47. Peng, Y. *et al.* Structures of the SARS-CoV-2 nucleocapsid and their perspectives for drug design. *EMBO J.* **39**, e105938 (2020).
48. Chen, C. Y. *et al.* Structure of the SARS Coronavirus Nucleocapsid Protein RNA-binding Dimerization Domain Suggests a Mechanism for Helical Packaging of Viral RNA. *J. Mol. Biol.* **368**, 1075–1086 (2007).
49. Duarte, M. *et al.* Telmisartan for treatment of Covid-19 patients: An open multicenter randomized clinical trial. *EClinicalMedicine* **37**, (2021).
50. Bai, Z., Cao, Y., Liu, W. & Li, J. The SARS-CoV-2 Nucleocapsid Protein and Its Role in Viral Structure, Biological Functions, and a Potential Target for Drug or Vaccine Mitigation. *Viruses* **13**, (2021).
51. Wohl, D. A. *et al.* Bictegravir combined with emtricitabine and tenofovir alafenamide versus dolutegravir, abacavir, and lamivudine for initial treatment of HIV-1 infection: week 96 results from a randomised, double-blind, multicentre, phase 3, non-inferiority trial. *lancet. HIV* **6**, e355–e363 (2019).
52. Gaur, A. H. *et al.* Fixed-dose combination bictegravir, emtricitabine, and tenofovir alafenamide in adolescents and children with HIV: week 48 results of a single-arm, open-label, multicentre, phase 2/3 trial. *Lancet. Child Adolesc. Heal.* **5**, 642–651

(2021).
53. Hong, H. *et al.* Identification of HIV-1 integrase inhibitors based on a four-point pharmacophore. *Antivir. Chem. Chemother.* **9**, 461–472 (1998).
54. Manerba, M. *et al.* Galloflavin (CAS 568-80-9): A Novel Inhibitor of Lactate Dehydrogenase. *ChemMedChem* **7**, 311–317 (2012).
55. Yamanaka, K. *et al.* A comprehensive strategy to discover inhibitors of the translesion synthesis DNA polymerase κ. *PLoS One* **7**, (2012).
56. Goebel, M., Clemenz, M. & Unger, T. Effective treatment of hypertension by AT(1) receptor antagonism: the past and future of telmisartan. *Expert Rev. Cardiovasc. Ther.* **4**, 615–629 (2006).
57. Nejat, R. *et al.* Losartan Inhibits SARS-CoV-2 Replication in Vitro. *J. Pharm. Pharm. Sci.* **24**, 390–399 (2021).
58. Grenningloh, R. *et al.* Cutting Edge: Inhibition of the Retinoid X Receptor (RXR) Blocks T Helper 2 Differentiation and Prevents Allergic Lung Inflammation. *J. Immunol.* **176**, 5161–5166 (2006).
59. Schulze, G. E. *et al.* BMS-189453, a Novel Retinoid Receptor Antagonist, Is a Potent Testicular Toxin. *Toxicol. Sci.* **59**, 297–308 (2001).
60. Varghese, E., Samuel, S. M., Liskova, A., Kubatka, P. & Büsselberg, D. Diabetes and coronavirus (SARS-CoV-2): Molecular mechanism of Metformin intervention and the scientific basis of drug repurposing. *PLOS Pathog.* **17**, e1009634 (2021).
61. Liu, L. Sen, Tanaka, H., Ishii, S. & Eckel, J. The New Antidiabetic Drug MCC-555 Acutely Sensitizes Insulin Signaling in Isolated Cardiomyocytes*This work was supported by the Ministerium für Wissenschaft und Forschung des Landes Nordrhein-Westfalen, the Bundesministerium für Gesundheit, EU COST Action B5, and a grant from Mitsubishi Chemical (Yokohama, Japan). *Endocrinology* **139**, 4531–4539 (1998).
62. Ramachandran, R. *et al.* TRPM8 activation attenuates inflammatory responses in mouse models of colitis. *Proc. Natl. Acad. Sci. U. S. A.* **110**, 7476–7481 (2013).
63. He, D. *et al.* Bisdemethoxycurcumin exerts a cell-protective effect via JAK2/STAT3 signaling in a rotenone-induced Parkinson's disease model in vitro. *Folia Histochem. Cytobiol.* **58**, 127–134 (2020).
64. Jiang, Y. *et al.* Structural analysis, virtual screening and molecular simulation to identify potential inhibitors targeting 2'-O-ribose methyltransferase of SARS-CoV-2 coronavirus. *J. Biomol. Struct. Dyn.* **40**, 1331–1346 (2022).
65. Liu, A. *et al.* New pharmaceuticals approved by FDA in 2020: Small-molecule drugs derived from amino acids and related compounds. *Chirality* **34**, 86–103 (2022).
66. Pooventhiran, T. *et al.* Energy and reactivity profile and proton affinity analysis of rimegepant with special reference to its potential activity against SARS-CoV-2 virus proteins using molecular dynamics. *J. Mol. Model.* **27**, (2021).
67. Ruilope, L. M. & Schumacher, H. Telmisartan 80 mg/hydrochlorothiazide 25 mg single-pill combination in the treatment of hypertension. *Expert Opin. Pharmacother.* **13**, 2417–2425 (2012).
68. Zhu, D. L. *et al.* Efficacy and tolerability of initial therapy with single-pill combination telmisartan/hydrochlorothiazide 80/25 mg in patients with grade 2 or 3 hypertension: a multinational, randomized, double-blind, active-controlled trial. *Clin. Ther.* **34**, 1613–1624 (2012).
69. Sun, X., Li, J., Li, Y., Wang, S. & Li, Q. Apatinib, a novel tyrosine kinase inhibitor, promotes ROS-dependent apoptosis and autophagy via the Nrf2/HO-1 pathway in Ovarian cancer cells. *Oxid. Med. Cell. Longev.* **2020**, (2020).
70. Giofrè, S. V. *et al.* Interaction of selected terpenoids with two SARS-CoV-2 key

therapeutic targets: An in silico study through molecular docking and dynamics simulations. *Comput. Biol. Med.* **134**, (2021).
71. Ribeiro, A. C. R. *et al.* Molecular mechanisms for the antidepressant-like effects of a low-dose ketamine treatment in a DFP-based rat model for Gulf War Illness. *Neurotoxicology* **80**, 52–59 (2020).
72. Chodroff, L., Bendele, M., Valenzuela, V., Henry, M. & Ruparel, S. EXPRESS: BDNF Signaling Contributes to Oral Cancer Pain in a Preclinical Orthotopic Rodent Model. *Mol. Pain* **12**, (2016).
73. Leggio, G. M. *et al.* Dopamine D3 Receptor Is Necessary for Ethanol Consumption: An Approach with Buspirone. *Neuropsychopharmacology* **39**, 2017 (2014).
74. Amati, F. *et al.* Hif1α down-regulation is associated with transposition of great arteries in mice treated with a retinoic acid antagonist. *BMC Genomics* **11**, 1–13 (2010).
75. Min, K. W., Zhang, X., Imchen, T. & Baek, S. J. A peroxisome proliferator-activated receptor ligand MCC-555 imparts anti-proliferative response in pancreatic cancer cells by PPARgamma-independent up-regulation of KLF4. *Toxicol. Appl. Pharmacol.* **263**, 225–232 (2012).
76. Sun, N., Lu, G., Lin, M., Fan, G. & Wu, Y. High-throughput quantification of a novel thiazolidinedione MCC-555 in rat plasma by ultra-fast liquid chromatography and its application in pharmacokinetic studies. *Talanta* **78**, 506–512 (2009).
77. Kou, M. C. *et al.* Curcuminoids distinctly exhibit antioxidant activities and regulate expression of scavenger receptors and heme oxygenase-1. *Mol. Nutr. Food Res.* **57**, 1598–1610 (2013).
78. Ponnusamy, S., Zinjarde, S., Bhargava, S., Rajamohanan, P. R. & Ravikumar, A. Discovering Bisdemethoxycurcumin from Curcuma longa rhizome as a potent small molecule inhibitor of human pancreatic α-amylase, a target for type-2 diabetes. *Food Chem.* **135**, 2638–2642 (2012).
79. Selescu, T., Ciobanu, A. C., Dobre, C., Reid, G. & Babes, A. Camphor activates and sensitizes transient receptor potential melastatin 8 (TRPM8) to cooling and icilin. *Chem. Senses* **38**, 563–575 (2013).
80. Tamayo, N. A. *et al.* Fused piperidines as a novel class of potent and orally available transient receptor potential melastatin type 8 (TRPM8) antagonists. *J. Med. Chem.* **55**, 1593–1611 (2012).
81. Holzer, P. Transient receptor potential (TRP) channels as drug targets for diseases of the digestive system. *Pharmacol. Ther.* **131**, 142 (2011).